ACS Photonics

pubs.acs.org/journal/apchd5

Article

Machine Learning Inverse Design of Topological Quantum States in Photonic Topological Insulators

Zhen Jiang,[‖] Yixin Wang,[‖] Bo Ji, Guangqiang He,* and Chun Jiang*

Cite This: *ACS Photonics* 2025, 12, 2566−2573

Read Online

ABSTRACT: Topological quantum optics has emerged as a promising platform for realizing robust quantum states due to its intrinsic topological protection. However, the complexity of band topologies presents significant challenges in designing devices capable of exciting tailored quantum states for specific applications. Here, we propose a machine learning-based inverse design approach for generating topological quantum states in photonic topological insulators. In our method, these quantum states are generated via four-wave mixing processes achieved through precise dispersion engineering of topological edge states. Our approach incorporates a tandem neural network architecture to facilitate the inverse design of kagome lattice structures within photonic crystals, using the Schmidt number as a critical performance metric. Moreover, we demonstrate that our deep learning framework effectively optimizes high-purity topological single-photon sources. This strategy offers a versatile and generalized method for tailoring topological quantum states, presenting significant potential to advance quantum information processing.

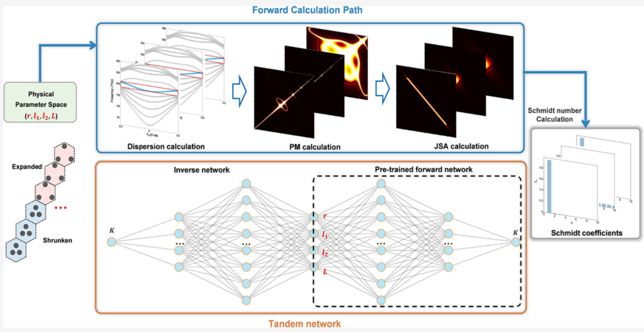

KEYWORDS: *topological quantum optics, inverse design, machine learning, entangled biphoton state, topological single-photon sources*

INTRODUCTION

Integrated quantum photonics has become a practical platform for next-generation data processing and communication, owing to its compatibility with integrated circuit fabrication technologies, high cost-effectiveness, and low-power consumption characteristics.[1,2] One of the key aspects of integrated quantum optics is the generation and manipulation of quantum sources.[3] However, quantum optical signals are fragile to decoherence and fidelity degradation in the presence of noise and structure imperfections.[4,5] Moreover, defects and irregularities are unavoidable during nanofabrication, making the development of robust quantum light sources essential for advancing integrated quantum devices.

At the same time, topological photonics offers a potential solution to the scalability problem of optical signals with its unique properties of unidirectional propagation, immunity to defects, and low loss.[6−12] As a result, topological photonics has been introduced into quantum systems, leading to breakthroughs such as topological quantum emitters,[13,14] topological entangled biphoton states,[5,15−17] topological quantum interference,[18,19] and topological quantum frequency combs.[20,21] Yet, efficiently generating specific quantum states in topological photonic crystals remains a challenge. This challenge arises from the band structure of photonic crystals, which is governed by their periodic configurations and inherent perturbations. The resulting intricate band topologies significantly complicate the design and optimization of topological quantum states.

Therefore, a key challenge in this field is finding effective strategies to solve the inverse problem of producing specific quantum states based on the dispersion properties of topological photonic crystals. Inverse design, a method that finds the best solutions within given constraints, offers significant convenience in the design of photonic devices.[22−29] Similar machine learning approaches have been applied in other engineering contexts.[30,31] However, while these optimization algorithms show attractive prospects, the study of the inverse design of topological quantum states remains unexplored.

Here we propose an inverse design method based on neural networks for designing photonic topological insulators to achieve the desired topological quantum states. In particular, we introduce a novel tandem neural network to address the challenging problem of both predicting and inversely designing topological quantum states. We demonstrate the presence of topological edge states localized at the interfaces between the

Received: December 26, 2024
Revised: April 1, 2025
Accepted: April 2, 2025
Published: April 8, 2025

https://doi.org/10.1021/acsphotonics.4c02592
ACS Photonics 2025, 12, 2566−2573

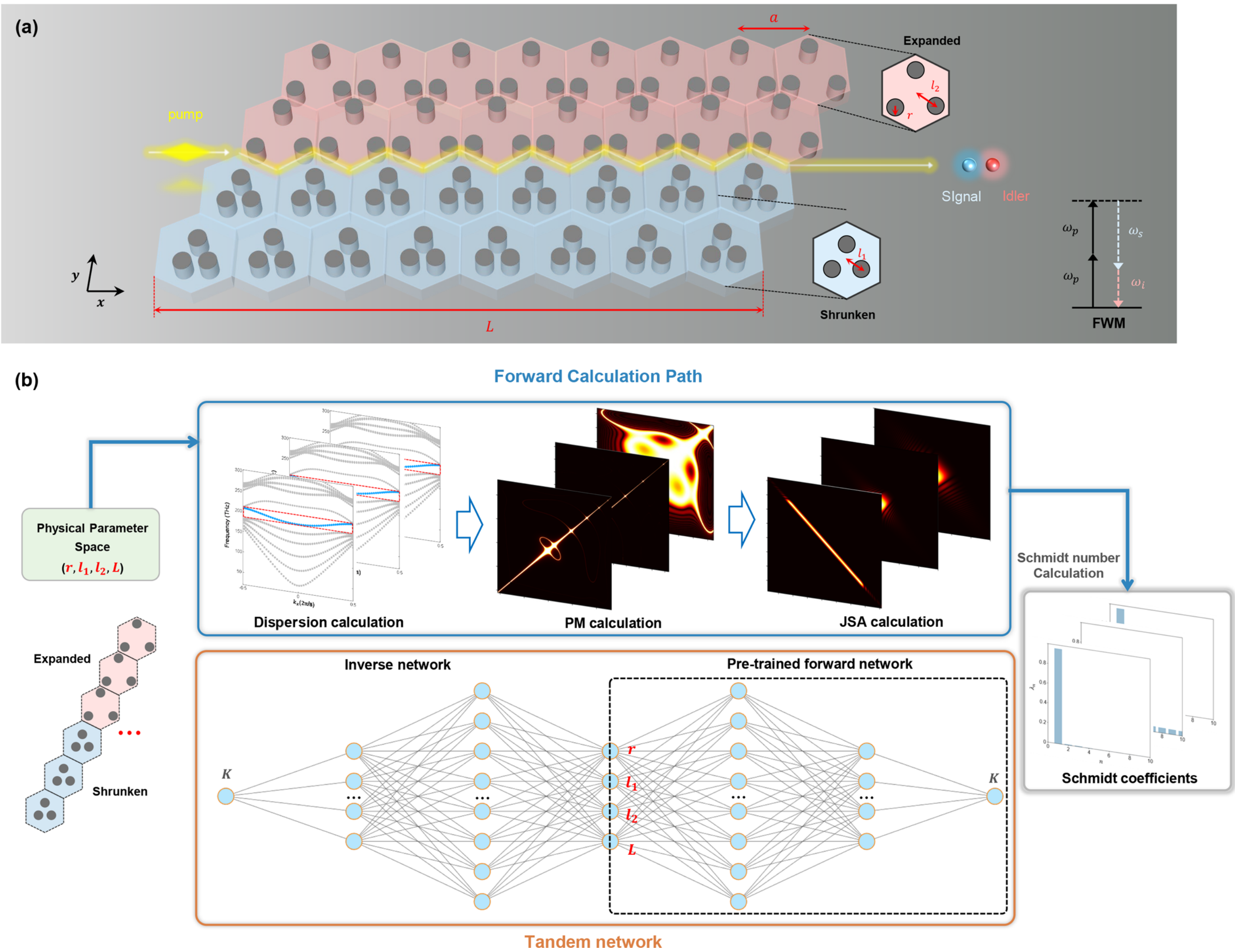

Figure 1. (a) Schematic illustration of a topological waveguide designed to support FWM processes, consisting of both shrunken and expanded kagome lattices. (b) Diagram of the inverse design methodology employing a tandem neural network, where an inverse network is coupled with a pretrained forward network to optimize topological quantum states.

shrunken and expanded kagome lattices. In kagome lattices, four-wave mixing (FWM) processes give rise to the generation of signal and idler photons. For physics-driven models, we introduce a constraint that ensures that the pump, signal, and idler frequencies remain within the operation bandwidth of the topological edge states. Consequently, these topological quantum states are inherently topologically protected, exhibiting robustness against sharp bends and structural imperfections. Specifically, the pretrained forward neural network (FNN) is used to predict the Schmidt number K, a key parameter quantifying the degree of entanglement in quantum states. And an inverse neural network (INN) is used to deduce the structural parameters of the kagome lattice required to achieve a target Schmidt number, thereby enabling a targeted design strategy in photonic crystal engineering. Furthermore, we demonstrate that our inverse design method can be applied to the design of high-purity topological single-photon sources. This approach to addressing inverse problems in topological quantum states offers considerable promise for advancing topological quantum optics, and provides novel perspectives and strategies.

RESULTS AND DISCUSSION

Topological Kagome Lattices. The kagome photonic lattice provides a practical platform for exhibiting topological edge states.[32−34] We consider an inverse design problem for topological quantum light sources in two-dimensional kagome lattices. As shown in Figure 1a, the topological waveguide is composed of two types of silicon-based kagome lattices with a lattice constant of a. The unperturbed kagome lattice, with its high symmetry, leads to a Dirac-like degeneracy at the K and K′ points in the Brillouin zone.[33] By deforming the unperturbed kagome lattice, two types of lattices can be obtained: a shrunken lattice (where the distance between the silicon cylinders and the center of the lattice is l_1) and an expanded lattice (where the distance is l_2). The deformation of kagome lattices leads to a complete photonic bandgap due to the breaking of perfect C_6 lattice symmetry.[32]

By applying the tight-binding model to the kagome lattice, the free Hamiltonian takes a form of[35]

$$\widehat{H}_0 = \begin{pmatrix} 0 & a_1 & b_1 \\ a_2 & 0 & c_1 \\ b_2 & c_2 & 0 \end{pmatrix} \tag{1}$$

https://doi.org/10.1021/acsphotonics.4c02592
ACS Photonics 2025, 12, 2566−2573

where the parameters are $a_1 = M + Je^{i(\frac{1}{2}k_x + \frac{\sqrt{3}}{2}k_y)a}$, $a_2 = M + Je^{-i(\frac{1}{2}k_x + \frac{\sqrt{3}}{2}k_y)a}$, $b_1 = M + Je^{-i(\frac{1}{2}k_x - \frac{\sqrt{3}}{2}k_y)a}$, $b_2 = M + Je^{i(\frac{1}{2}k_x - \frac{\sqrt{3}}{2}k_y)a}$, $c_1 = M + Je^{-ik_xa}$, $c_2 = M + Je^{ik_xa}$, M and J denote the intracell coupling and intercell coupling, respectively. The Hamiltonians transformed by the unitary chiral operator are given by $\hat{H}_1 = \Gamma_3 H_0 \Gamma_3^{-1}$ and $\hat{H}_2 = \Gamma_3 H_1 \Gamma_3^{-1}$, respectively, where Γ_3 is the unitary chiral operator with eigenvalues of 0, $e^{i2\pi/3}$, and $e^{-i2\pi/3}$.[34] Therefore, we can find $\hat{H}_0 + \hat{H}_1 + \hat{H}_2 = 0$, which reveals the generalized chiral symmetry of the kagome lattices. This Hamiltonian is analogous to the Hamiltonian of the topological Su−Schrieffer−Heeger (SSH) model.

The band topology of kagome lattices can be described by the bulk polarization, which is given by[36]

$$p_s = 1/N_k \sum_{j,k_t} v_s^j(k_t) \tag{2}$$

where $v_s^j(k_t)$ is the eigenvalue (also referred to as Wannier center) of the Wilson loop. The Wilson loop's eigenvalue problem is given by $W_{k_s+2\pi \leftarrow k_s,k_t}|\nu_k\rangle^j = e^{i2\pi v_s^j(k_t)}|\nu_k\rangle^j$, where k_s, $k_t = 0, \delta k, \cdots, (N_k - 1)\delta k$, $\delta k = \frac{1}{N_k}\frac{4\pi}{\sqrt{3}a}$ and j is the index of the occupied bands. Note that the bulk polarization of shrunken lattices is calculated as 0 (indicating a trivial case), while the calculated bulk polarization of expanded lattices is 1/3 (indicating a nontrivial case).[34] According to the bulk−boundary correspondence, the polarization difference leads to topological edge states localized at the boundaries between the shrunken and expanded kagome lattices.

Topological Quantum States. Due to the third-order nonlinearity of silicon, the nonlinear FWM processes generated in the topological waveguide could lead to entangled biphoton states.[5,15,16] The energy and momentum conservation in the FWM processes are described by the equations: $2\omega_p = \omega_s + \omega_i$ and $2k_p = k_s + k_i$. Here, $\omega_{p,s,i}$ are the frequencies and $k_{p,s,i}$ are the wavevectors of the pump, signal, and idler, respectively. The dynamics of the FWM process originate from the nonlinear Hamiltonian, which is given by

$$\hat{H}_{NL} \approx -\hbar\gamma(\hat{a}_s^\dagger \hat{a}_i^\dagger \hat{a}_p \hat{a}_p + \hat{a}_p^\dagger \hat{a}_p^\dagger \hat{a}_s \hat{a}_i) \tag{3}$$

where γ is the nonlinear strength, $\hat{a}_{s,i}^\dagger$ and $\hat{a}_{s,i}$ are creation and annihilation operators, respectively. The generated biphoton state can be written as

$$|\Psi\rangle = \iint d\omega_s d\omega_i \mathcal{A}(\omega_s, \omega_i)\hat{a}_s^\dagger(\omega_s)\hat{a}_i^\dagger(\omega_i)|0\rangle \tag{4}$$

where $\mathcal{A}(\omega_s, \omega_i)$ is the joint spectral amplitude (JSA). The JSA is determined by

$$\mathcal{A}(\omega_s, \omega_i) = \alpha\left(\frac{\omega_s + \omega_i}{2}\right)\mathrm{sinc}\left(\frac{\Delta kL}{2}\right) \tag{5}$$

where $\alpha\left(\frac{\omega_s + \omega_i}{2}\right)$ represents the pump spectrum, and $\mathrm{sinc}\left(\frac{\Delta kL}{2}\right)$ is the joint phase-matching (PM) spectrum, and $\Delta k = 2k_p - k_s - k_i$ is the phase mismatch.[37]

The generation of the FWM process in topological devices depends on specific PM conditions, which are determined by the dispersion of topological edge states.[15] A key challenge here is how to excite nonlinear FWM processes by controlling the dispersion of topological edge states. In topological structures, we can modify the dispersion of edge states by adjusting structural parameters like geometry, size, and rod arrangement.

To analyze the separability of the biphoton state, JSA can be decomposed as

$$\mathcal{A}(\omega_s, \omega_i) = \sum_{n=1}^{N} \sqrt{\lambda_n}\psi_n(\omega_s)\phi_n(\omega_i) \tag{6}$$

where λ_n ($N \in \mathbb{N}$) is the Schmidt coefficient, ψ_n and ϕ_n are orthonormal functions of ω_s and ω_i in the Hilbert space. The presence of nonzero Schmidt coefficients (greater than 1) indicates the biphoton state is frequency entangled, rather than a simple separable state. Furthermore, the entanglement entropy S_k can be calculated from the Schmidt coefficients:

$$S_k = -\sum_{n=1}^{N} \lambda_n \log_2 \lambda_n \tag{7}$$

And the Schmidt number K also can be used to quantify the degree of entanglement[38]

$$K = \left(\sum_{n=1}^{N} \lambda_n\right)^2 / \sum_{n=1}^{N} \lambda_n^2 \tag{8}$$

Also, we can access the joint temporal amplitude (JTA) of biphotons from the Fourier transform of the JSA $\mathcal{A}(t_s, t_i) = \mathcal{F}[\mathcal{A}(\omega_i, \omega_s)]$.[27]

With the Schmidt decomposition, the single-photon purity of the biphoton state can be obtained. Single-photon purity is crucial for achieving high visibility quantum interference between photons from the same source. Typically, single-photon purity is represented by $\mathrm{Tr}(\hat{\rho}_s^2)$, where $\hat{\rho}_s = \mathrm{Tr}(|\Psi\rangle\langle\Psi|)$ is the density operator for the heralded single photon, and Tr is the trace over the idler mode. Then we can calculate the single-photon purity as[39]

$$\mathcal{P} = K^{-1} = \sum_{n=1}^{N} \lambda_n^2 / \left(\sum_{n=1}^{N} \lambda_n\right)^2 \tag{9}$$

Note that the $\mathcal{P} = 1$ denotes a separable quantum state: $\mathcal{A}(\omega_s, \omega_i) = f_s(\omega_s)f_i(\omega_i)$. These spectrum-uncorrelated photons are shown to be applicable to boson sampling and quantum information processing.[37,40]

Deep Learning Method. Although a specific optical structure corresponds to only one type of band dispersion and generates the corresponding quantum state under certain pump conditions (a one-to-one relationship), a single type of band dispersion may correspond to multiple optical structures, leading to a one-to-many problem. This ambiguity adds complexity to the inverse design of optical structures. A tandem architecture,[23,41−43] which combines forward and inverse neural networks, offers an effective solution to this challenge.

Given that a specific band dispersion can correspond to multiple optical structures, we employ a tandem neural network architecture. This approach integrates a pretrained forward model into the inverse design process, ensuring that predicted structures are physically valid. Instead of directly mapping band dispersion to structural parameters, the inverse model generates an initial design, which is then verified by the forward model to minimize the discrepancy between the computed and target dispersion. This strategy effectively

https://doi.org/10.1021/acsphotonics.4c02592
ACS Photonics 2025, 12, 2566−2573

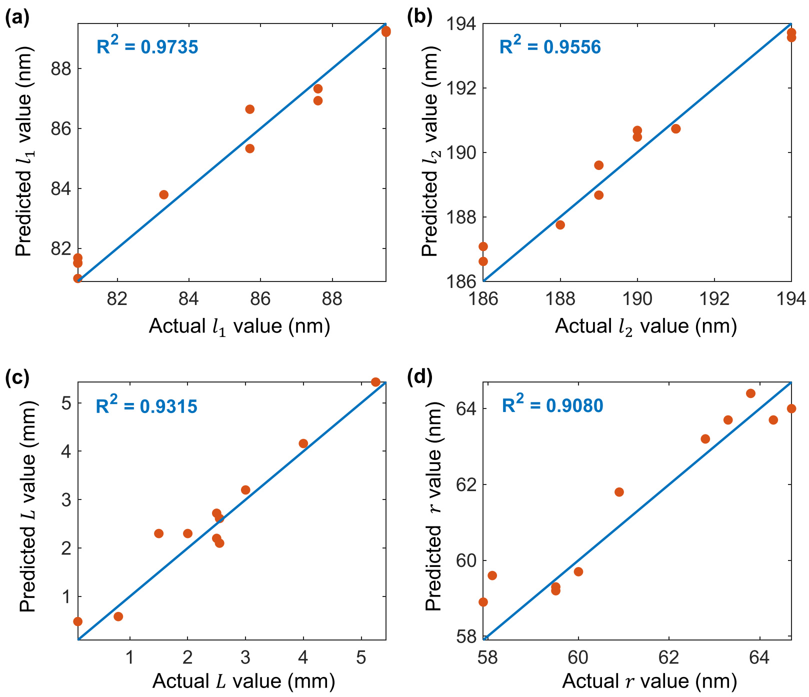

Figure 2. (a−d) Predicted and actual values (FDTD-based) across four kagome lattice parameters: l_1, l_2, L, and r, respectively.

mitigates ambiguity, stabilizes training, and enhances the generalization ability of our model.

As shown in the lower part of Figure 1b, our tandem neural network is composed of two interconnected subnetworks: a pretrained FNN and an INN. The tandem network generates the predicted parameters based on the designed structure. The FNN with 5 hidden layers is pretrained to predict the Schmidt number K from the input structural parameters, and its weights are subsequently fixed. And the INN with 2 hidden layers is designed to map the Schmidt number K back to the corresponding kagome lattice parameters. In particular, the INN is trained to minimize a cost function defined as the error between the predicted and target responses. Initially, we define the individual optimization parameters for the kagome lattices, including the structural parameters l_1, l_2, L, and r, where L is the length of the topological waveguide.

The data set used in this study consists of 3000 training instances and 50 test instances generated from finite-difference time-domain (FDTD) simulations. In the FDTD simulations, the band structure of the topological kagome lattices is computed based on given structural parameters. By extracting the dispersion curves of the topological edge states, we obtain the PM intensity of the FWM processes. The pump light is a Gaussian pulse with a center frequency of 193.5 THz and a full width at half-maximum (FWHM) of 5 nm. Using the pump equation $\alpha\left(\frac{\omega_s + \omega_i}{2}\right)$ and the phase matching term PM, we can compute the JSA of the biphoton state. With the Schmidt decomposition, Schmidt number K of topological quantum states can be calculated.

We focus on the convergence behavior of the training process, the accuracy of the predicted parameters, and the comparison of the results with the FDTD simulations. After training the model with the optimal parameters, we evaluated its performance on a separate test data set. As shown in Figure 2, we present the predicted and actual values of four key kagome lattice parameters (l_1, l_2, L, and r) obtained by an FDTD-based approach. The regression analysis yields R^2 values above 0.9 for all parameters. This high degree of correlation between the predicted and actual values demonstrates that our machine learning method reliably captures the underlying relationships in the data. Consequently, these results validate the feasibility and effectiveness of our proposed machine learning framework in predicting the geometric parameters of kagome lattices.

To validate the practical applicability of our model's predictions, we select 10 input features from the test data set and feed them into the trained model to obtain 10 predicted structural parameters. These predicted parameters are then used in a numerical simulation platform to calculate the corresponding Schmidt number K values. As shown in Figure 3, the comparison between the target K values and those calculated from the predicted parameters yields an R^2 value of 0.9763. This high degree of correlation indicates that the entanglement properties K obtained from the predicted structural parameters are in excellent agreement with the

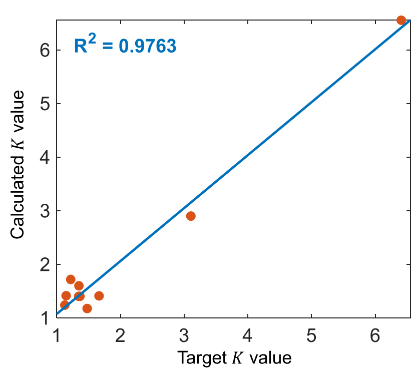

Figure 3. Comparison of the target K values (from the test data set) with the K values calculated using the parameters predicted by the machine learning model.

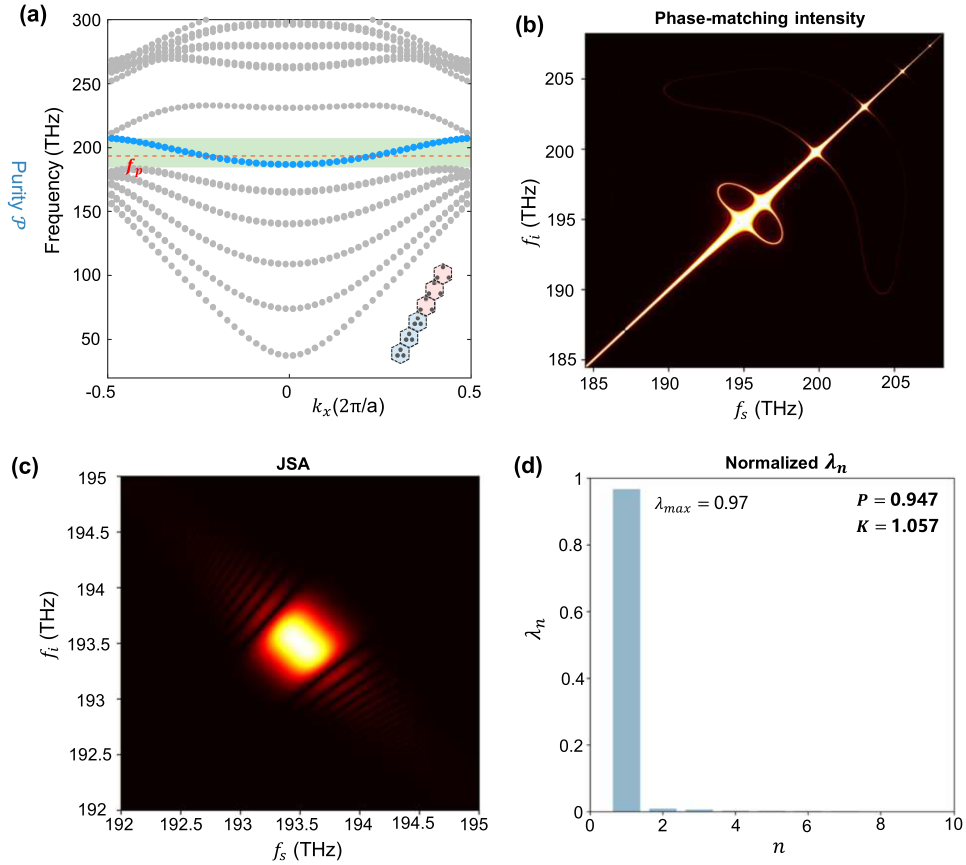

Figure 4. Deep learning design results of high-purity topological single-photon sources with certain pumping. (a) Band structure of the topological kagome lattices, where the green area represents the operation bandwidth of topological edge states, f_p is the frequency of the pump. (b) PM intensity of FWM processes generated in topological waveguides. (c) JSA and (d) Schmidt coefficients λ_n of biphoton states generated in topological waveguides.

actual values. Our model thus performs remarkably well on the test data set, demonstrating strong generalization capabilities and confirming the feasibility of our machine learning approach to accurately predict structural parameters.

Inverse Design for High-Purity Topological Single-Photon Sources. To evaluate the effectiveness of the inverse design process in predicting the structural parameters of the kagome lattice, we consider an inverse design problem for high-purity topological single-photon sources using our tandem neural network. Single-photon sources are devices that emit and control individual photons, which play crucial roles in quantum information processing and quantum communications.[37,40,44] Especially, heralded single-photon sources are quantum sources whose existence is "announced" in some way when a single photon is generated.[37,45]

To achieve high-purity topological single-photon sources, it is crucial to optimize the structural parameters L and Δk (extracted from the dispersion curve of the topological edge state). A Schmidt number of $K = 1$ indicates that the quantum state is an ideal single-photon source, with $\mathcal{P} = 1$ denoting maximum single-photon purity.[39] In practice, generating a perfect single-photon source using topological quantum states in the kagome lattice structure is extremely challenging. The distinctive dispersion characteristics of topological edge states lead to the complexity of PM design. We first consider the high-purity single-photon source with a target: $K = 1.05$ by our deep learning method. The predicted parameter values of kagome lattices are $l_1 = 0.170a$, $l_2 = 0.402a$, $L = 2.25$ mm, $r = 0.126a$, respectively.

Using these predicted parameters, we can calculate the band structure of the topological kagome lattices, as shown in Figure 4a. Within the photonic bandgap, there exists a pair of topological edge states, with the frequency of the pump aligning with the operational bandwidth.[15] The PM intensity of FWM processes $\mathrm{PM} = \mathrm{sinc}\left(\frac{\Delta k L}{2}\right)$ is shown in Figure 4b. Using the pump equation $\alpha\left(\frac{\omega_s + \omega_i}{2}\right)$ and the phase matching term PM, we can compute the JSA of the biphoton state as shown in Figure 4c. With our deep learning method, the JSA is optimized to be close to a round shape form. The signal and idler photons have similar bandwidths and operate as near-indistinguishable biphotons over a wide spectral range.[37,45−47] The Schmidt coefficients λ_n, obtained from Schmidt decomposition, are displayed in Figure 4d, with the largest normalized Schmidt coefficient $\lambda_n = 0.97$, indicating weak entanglement of the quantum state.[38]

Further, we calculate the Schmidt number $K = 1.057$, denoting a single-photon purity of $\mathcal{P} = 0.947$. This result implies an ultrahigh-purity topological single-photon source by our inverse design method. Notably, due to the specific shapes of the dispersion curves for the topological edge states and the limits of precision in nanofabrication processing, achieving near-perfect single-photon purity in topological quantum light sources is challenging. Despite these limitations, it is still an optimal solution under the current constraints. Also, compared

https://doi.org/10.1021/acsphotonics.4c02592
ACS Photonics 2025, 12, 2566−2573

to traditional inverse learning methods, our machine learning method offers significant advantages in computational efficiency and scalability (see Supporting Information).

Robustness against Disorders for FWM Processes. To verify the topological protection of topological edge states, we simulate the field profiles in kagome lattices with defects employing COMSOL Multiphysics software. We consider a scheme of a topological waveguide composed of shrunken and expanded kagome lattices, where the parameters are obtained according to the optimization results (Figure 4). In our numerical model, a point source positioned at the input port is used to excite topological edge states. As shown in Figure 5a,

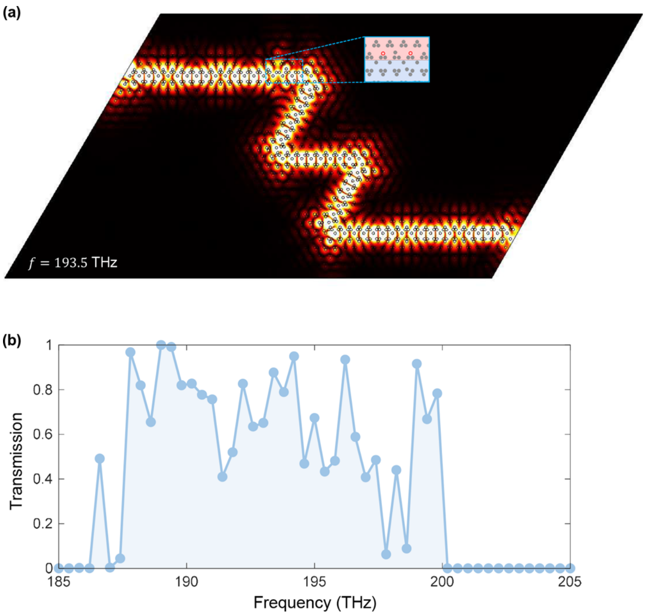

Figure 5. (a) Field profiles and (b) simulated transmission spectrum of topological edge states in kagome lattice.

within the blue area, several rods are randomly moved by distances between $-0.1a$ and $0.2a$, and two rods are removed. Figure 5b shows the simulated transmission spectrum of the edge state in this topological waveguide. We can clearly observe a bandwidth of topological edge states, where the transmission efficiency can approach unity. However, outside the bandwidth, the transmission efficiency drops dramatically because topological edge states are not supported in these frequencies. Most importantly, the excited edge modes are robust against sharp bends and defects due to the topological nature of the edge states. Since all the frequencies of FWM processes are within the operation bandwidth of topological edge states, the quantum states generated in kagome lattices are inborn topologically protected.[15,48]

CONCLUSIONS

We propose a novel machine learning-based inverse design method for engineering topological quantum states in photonic topological insulators. By exploiting the unique dispersion properties of topological edge states localized at the interfaces between shrunken and expanded kagome lattices, our approach enables the generation of robust quantum states via FWM processes. The tandem neural network—integrating a pretrained forward network to predict the Schmidt number and an inverse network to determine the optimal structural parameters—provides a powerful tool for tailoring quantum states to specific target properties. Notably, we have demonstrated the design of a topological single-photon source achieving a purity of 0.947, highlighting the potential of our method for realizing high-performance quantum devices. While our current implementation is based on kagome lattice configurations, the versatility of this inverse design strategy paves the way for its application to a broader range of photonic crystal structures. By significantly reducing the design complexity inherent in topological photonic systems, our work not only advances the state-of-the-art in topological quantum optics but also opens new avenues for robust quantum information processing in integrated photonic platforms.

METHODS

Optimization Details. Our deep learning approach is implemented in Python, using some key libraries to build and train neural networks. In particular, we use TensorFlow—a widely used deep learning framework—to define and train both the forward and inverse neural networks. Our inverse design process is executed on a computer equipped with an Intel(R) Xeon(R) W-2255 CPU @3.70 GHz and 128 GB of RAM. In the FDTD settings, the kagome lattices are formed by the silicon cylinders (ϵ = 12) in the air background (ϵ_0 = 1).

ASSOCIATED CONTENT

Supporting Information

The Supporting Information is available free of charge at https://pubs.acs.org/doi/10.1021/acsphotonics.4c02592.

Genetic algorithm (GA)-based inverse design approach; experimental realization of quantum states in topological photonic crystals (PDF)

AUTHOR INFORMATION

Corresponding Authors

Guangqiang He − *State Key Laboratory of Photonics and Communications, Department of Electronic Engineering, Shanghai Jiao Tong University, Shanghai 200240, China;* orcid.org/0000-0001-9017-4159; Email: gqhe@sjtu.edu.cn

Chun Jiang − *State Key Laboratory of Photonics and Communications, Department of Electronic Engineering, Shanghai Jiao Tong University, Shanghai 200240, China;* orcid.org/0000-0003-1873-6385; Email: cjiang@sjtu.edu.cn

Authors

Zhen Jiang − *State Key Laboratory of Photonics and Communications, Department of Electronic Engineering, Shanghai Jiao Tong University, Shanghai 200240, China; State Key Laboratory of Photonics and Communications, School of Electronics, Peking University, Beijing 100871, China*

Yixin Wang − *State Key Laboratory of Photonics and Communications, Department of Electronic Engineering, Shanghai Jiao Tong University, Shanghai 200240, China; College of Big Data and Information Engineering, Institute of New Optoelectronic Materials and Technology, Guizhou University, Guiyang 550025, China*

https://doi.org/10.1021/acsphotonics.4c02592
ACS Photonics 2025, 12, 2566−2573

Bo Ji – *State Key Laboratory of Photonics and Communications, Department of Electronic Engineering, Shanghai Jiao Tong University, Shanghai 200240, China*

Complete contact information is available at:
https://pubs.acs.org/10.1021/acsphotonics.4c02592

Author Contributions

[‖]Z.J. and Y.W. contributed equally to this work.

Notes

The authors declare no competing financial interest.

■ ACKNOWLEDGMENTS

This work is supported by the National Key Research and Development Program of China (2021YFB2800401), the National Natural Science Foundation of China (62075129), the Postdoctoral Fellowship Program of CPSF (GZC20240059), and the Sichuan Provincial Key Laboratory of Microwave Photonics (2023-04).

■ REFERENCES

(1) Wang, Y.; Jöns, K. D.; Sun, Z. Integrated photon-pair sources with nonlinear optics. *Appl. Phys. Rev.* **2021**, *8*, No. 011314.

(2) Caspani, L.; Xiong, C.; Eggleton, B. J.; Bajoni, D.; Liscidini, M.; Galli, M.; Morandotti, R.; Moss, D. J. Integrated sources of photon quantum states based on nonlinear optics. *Light: Science & Applications* **2017**, *6*, e17100−e17100.

(3) Moody, G.; Chang, L.; Steiner, T. J.; Bowers, J. E. Chip-scale nonlinear photonics for quantum light generation. *AVS Quantum Sci.* **2020**, *2*, No. 041702.

(4) Omran, A.; Levine, H.; Keesling, A.; Semeghini, G.; Wang, T. T.; Ebadi, S.; Bernien, H.; Zibrov, A. S.; Pichler, H.; Choi, S.; et al. Generation and manipulation of Schrödinger cat states in Rydberg atom arrays. *Science* **2019**, *365*, 570−574.

(5) Dai, T.; Ao, Y.; Bao, J.; Mao, J.; Chi, Y.; Fu, Z.; You, Y.; Chen, X.; Zhai, C.; Tang, B.; et al. Topologically protected quantum entanglement emitters. *Nat. Photonics* **2022**, *16*, 248−257.

(6) Haldane, F. D. M.; Raghu, S. Possible realization of directional optical waveguides in photonic crystals with broken time-reversal symmetry. *Phys. Rev. Lett.* **2008**, *100*, No. 013904.

(7) Raghu, S.; Haldane, F. D. M. Analogs of quantum-Hall-effect edge states in photonic crystals. *Phys. Rev. A* **2008**, *78*, No. 033834.

(8) Cheng, X.; Jouvaud, C.; Ni, X.; Mousavi, S. H.; Genack, A. Z.; Khanikaev, A. B. Robust reconfigurable electromagnetic pathways within a photonic topological insulator. *Nat. Mater.* **2016**, *15*, 542−548.

(9) Wu, L.-H.; Hu, X. Scheme for achieving a topological photonic crystal by using dielectric material. *Phys. Rev. Lett.* **2015**, *114*, No. 223901.

(10) Slobozhanyuk, A.; Mousavi, S. H.; Ni, X.; Smirnova, D.; Kivshar, Y. S.; Khanikaev, A. B. Three-dimensional all-dielectric photonic topological insulator. *Nat. Photonics* **2017**, *11*, 130−136.

(11) Yang, Y.; Yamagami, Y.; Yu, X.; Pitchappa, P.; Webber, J.; Zhang, B.; Fujita, M.; Nagatsuma, T.; Singh, R. Terahertz topological photonics for on-chip communication. *Nat. Photonics* **2020**, *14*, 446−451.

(12) Wu, H.; Xu, H.; Xie, L.; Jin, L. Edge state, band topology, and time boundary effect in the fine-grained categorization of chern insulators. *Phys. Rev. Lett.* **2024**, *132*, No. 083801.

(13) Mittal, S.; Goldschmidt, E. A.; Hafezi, M. A topological source of quantum light. *Nature* **2018**, *561*, 502−506.

(14) Barik, S.; Karasahin, A.; Flower, C.; Cai, T.; Miyake, H.; DeGottardi, W.; Hafezi, M.; Waks, E. A topological quantum optics interface. *Science* **2018**, *359*, 666−668.

(15) Jiang, Z.; Ding, Y.; Xi, C.; He, G.; Jiang, C. Topological protection of continuous frequency entangled biphoton states. *Nanophotonics* **2021**, *10*, 4019−4026.

(16) Afzal, S.; Zimmerling, T. J.; Rizvandi, M.; Taghavi, M.; Esmaeilifar, L.; Hrushevskyi, T.; Kaur, M.; Van, V.; Barzanjeh, S. Enhanced quantum emission from a topological Floquet resonance. *PRX Quantum* **2024**, *5*, No. 040331.

(17) Jiang, Z.; Ji, B.; Chen, Y.; Jiang, C.; He, G. Manipulating multiple optical parametric processes in photonic topological insulators. *Phys. Rev. B* **2024**, *109*, No. 174110.

(18) Mittal, S.; Orre, V. V.; Goldschmidt, E. A.; Hafezi, M. Tunable quantum interference using a topological source of indistinguishable photon pairs. *Nat. Photonics* **2021**, *15*, 542−548.

(19) Chen, Y.; He, X.-T.; Cheng, Y.-J.; Qiu, H.-Y.; Feng, L.-T.; Zhang, M.; Dai, D.-X.; Guo, G.-C.; Dong, J.-W.; Ren, X.-F. Topologically protected valley-dependent quantum photonic circuits. *Phys. Rev. Lett.* **2021**, *126*, No. 230503.

(20) Jiang, Z.; Chen, Y.; Jiang, C.; He, G. Generation of Quantum Optical Frequency Combs in Topological Resonators. *Adv. Quantum Technol.* **2024**, *7*, No. 2300354.

(21) Jiang, Z.; Wang, H.; Xie, P.; Yang, Y.; Shen, Y.; Ji, B.; Chen, Y.; Zhang, Y.; Sun, L.; Wang, Z.; et al. On-chip topological transport of integrated optical frequency combs. *Photonics Research* **2025**, *13*, 163−176.

(22) Molesky, S.; Lin, Z.; Piggott, A. Y.; Jin, W.; Vucković, J.; Rodriguez, A. W. Inverse design in nanophotonics. *Nat. Photonics* **2018**, *12*, 659−670.

(23) Liu, D.; Tan, Y.; Khoram, E.; Yu, Z. Training deep neural networks for the inverse design of nanophotonic structures. *ACS Photonics* **2018**, *5*, 1365−1369.

(24) Liu, Z.; Zhu, D.; Raju, L.; Cai, W. Tackling photonic inverse design with machine learning. *Adv. Sci.* **2021**, *8*, No. 2002923.

(25) Long, Y.; Ren, J.; Li, Y.; Chen, H. Inverse design of photonic topological state via machine learning. *Appl. Phys. Lett.* **2019**, *114*, 181105.

(26) Yang, J.; Guidry, M. A.; Lukin, D. M.; Yang, K.; Vučković, J. Inverse-designed silicon carbide quantum and nonlinear photonics. *Light: Sci. Appl.* **2023**, *12*, 201.

(27) Cai, W.-H.; Tian, Y.; Wang, S.; You, C.; Zhou, Q.; Jin, R.-B. Optimized Design of the Lithium Niobate for Spectrally-Pure-State Generation at MIR Wavelengths Using Metaheuristic Algorithm. *Adv. Quantum Technol.* **2022**, *5*, No. 2200028.

(28) Yang, K. Y.; Shirpurkar, C.; White, A. D.; Zang, J.; Chang, L.; Ashtiani, F.; Guidry, M. A.; Lukin, D. M.; Pericherla, S. V.; Yang, J.; et al. Multi-dimensional data transmission using inverse-designed silicon photonics and microcombs. *Nat. Commun.* **2022**, *13*, 7862.

(29) Yang, K. Y.; Skarda, J.; Cotrufo, M.; Dutt, A.; Ahn, G. H.; Sawaby, M.; Vercruysse, D.; Arbabian, A.; Fan, S.; Alù, A.; et al. Inverse-designed non-reciprocal pulse router for chip-based LiDAR. *Nat. Photonics* **2020**, *14*, 369−374.

(30) Li, B.; Zhu, J.; Zhao, X.; Yao, H. Residual stress prediction in laser shock peening induced LD-TC4 alloy by data-driven ensemble learning methods. *Optics & Laser Technology* **2024**, *176*, No. 110946.

(31) Li, B.; Zhu, J.; Zhao, X. A hybrid physics informed predictive scheme for predicting low-cycle fatigue life and reliability of aerospace materials under multiaxial loading conditions. *Reliability Engineering & System Safety* **2025**, *257*, No. 110838.

(32) Vakulenko, A.; Kiriushechkina, S.; Wang, M.; Li, M.; Zhirihin, D.; Ni, X.; Guddala, S.; Korobkin, D.; Alù, A.; Khanikaev, A. B. Near-field characterization of higher-order topological photonic states at optical frequencies. *Adv. Mater.* **2021**, *33*, No. 2004376.

(33) Li, M.; Zhirihin, D.; Gorlach, M.; Ni, X.; Filonov, D.; Slobozhanyuk, A.; Alù, A.; Khanikaev, A. B. Higher-order topological states in photonic kagome crystals with long-range interactions. *Nat. Photonics* **2020**, *14*, 89−94.

(34) Ezawa, M. Higher-order topological insulators and semimetals on the breathing kagome and pyrochlore lattices. *Phys. Rev. Lett.* **2018**, *120*, No. 026801.

(35) Ni, X.; Weiner, M.; Alu, A.; Khanikaev, A. B. Observation of higher-order topological acoustic states protected by generalized chiral symmetry. *Nat. Mater.* **2019**, *18*, 113−120.

(36) King-Smith, R.; Vanderbilt, D. Theory of polarization of crystalline solids. *Phys. Rev. B* **1993**, *47*, 1651.
(37) Mosley, P. J.; Lundeen, J. S.; Smith, B. J.; Wasylczyk, P.; U'Ren, A. B.; Silberhorn, C.; Walmsley, I. A. Heralded generation of ultrafast single photons in pure quantum states. *Phys. Rev. Lett.* **2008**, *100*, No. 133601.
(38) Law, C.; Walmsley, I. A.; Eberly, J. Continuous frequency entanglement: effective finite Hilbert space and entropy control. *Phys. Rev. Lett.* **2000**, *84*, 5304.
(39) Vicent, L. E.; U'Ren, A. B.; Rangarajan, R.; Osorio, C. I.; Torres, J. P.; Zhang, L.; Walmsley, I. A. Design of bright, fiber-coupled and fully factorable photon pair sources. *New J. Phys.* **2010**, *12*, No. 093027.
(40) Niu, M. Y.; Chuang, I. L.; Shapiro, J. H. Qudit-basis universal quantum computation using χ (2) interactions. *Phys. Rev. Lett.* **2018**, *120*, No. 160502.
(41) Gostimirovic, D.; Grinberg, Y.; Xu, D.-X.; Liboiron-Ladouceur, O. Improving fabrication fidelity of integrated nanophotonic devices using deep learning. *ACS Photonics* **2023**, *10*, 1953−1961.
(42) Wu, B.; Ding, K.; Chan, C. T.; Chen, Y. Machine prediction of topological transitions in photonic crystals. *Physical Review Applied* **2020**, *14*, No. 044032.
(43) Pilozzi, L.; Farrelly, F. A.; Marcucci, G.; Conti, C. Machine learning inverse problem for topological photonics. *Commun. Phys.* **2018**, *1*, 57.
(44) Sun, Q.-C.; Jiang, Y.-F.; Mao, Y.-L.; You, L.-X.; Zhang, W.; Zhang, W.-J.; Jiang, X.; Chen, T.-Y.; Li, H.; Huang, Y.-D.; et al. Entanglement swapping over 100 km optical fiber with independent entangled photon-pair sources. *Optica* **2017**, *4*, 1214−1218.
(45) Brańczyk, A. M.; Fedrizzi, A.; Stace, T. M.; Ralph, T. C.; White, A. G. Engineered optical nonlinearity for quantum light sources. *Opt. Express* **2011**, *19*, 55−65.
(46) Hong, C.-K.; Ou, Z.-Y.; Mandel, L. Measurement of subpicosecond time intervals between two photons by interference. *Phys. Rev. Lett.* **1987**, *59*, 2044.
(47) Santori, C.; Fattal, D.; Vučković, J.; Solomon, G. S.; Yamamoto, Y. Indistinguishable photons from a single-photon device. *Nature* **2002**, *419*, 594−597.
(48) You, J. W.; Lan, Z.; Panoiu, N. C. Four-wave mixing of topological edge plasmons in graphene metasurfaces. *Sci. Adv.* **2020**, *6*, No. eaaz3910.

https://doi.org/10.1021/acsphotonics.4c02592
ACS Photonics 2025, 12, 2566−2573

Supplementary Information: Machine learning inverse design of topological quantum states in photonic topological insulators

Zhen Jiang[a,b,#], Yixin Wang[a,c,#], Bo Ji[a], Guangqiang He[a,*] and Chun Jiang[a†]
[a] *State Key Laboratory of Photonics and Communications, Department of Electronic Engineering, Shanghai Jiao Tong University, Shanghai 200240, China*
[b] *State Key Laboratory of Photonics and Communications, School of Electronics, Peking University, Beijing 100871, China*
[c] *College of Big Data and Information Engineering, Institute of New Optoelectronic Materials and Technology, Guizhou University, Guiyang 550025, China*
[#] *These authors contributed equally to this work.*

I. GENETIC ALGORITHM (GA)-BASED INVERSE DESIGN APPROACH

In this section, we compare a genetic algorithm (GA)-based inverse design with our machine learning (ML)-based approach, focusing on accuracy and computational efficiency. The GA is a widely used evolutionary optimization method inspired by natural selection. In this study, we employ GA to optimize kagome lattices for generating topological quantum states. The workflow of our GA-based inverse design approach is illustrated in Fig. S1(a). Initially, we also define the structural parameters l_1, l_2, L, and r. The optimization process relies on a well-defined fitness function, which evaluates the quality of each potential solution. Specifically, our fitness function integrates MEEP-based photonic band structure simulations and single-photon purity calculations to determine the optimal design parameters.

The GA-based inverse design process begins with setting up the initial population of kagome lattice structures, where each individual is characterized by a specific set of design parameters. The goal of GA is to identify structural parameters that optimize the fitness function , which is defined based on the purity of the single-photon source. In our optimization process, we define this fitness as

$$\mathbf{O}_{target} = \left(\sum_{n=1}^{N} \lambda_n\right)^2 / \sum_{n=1}^{N} \lambda_n^2 - 1. \tag{S1}$$

During optimization, a new generation of candidate structures is iteratively produced through selection, crossover, and mutation operations. To enhance convergence efficiency, a tournament selection strategy is employed, which retains the top-performing individuals (5% of the population size) to progress to the next generation without undergoing genetic operations. This approach helps mitigate premature convergence to local optima. The GA terminates when the convergence threshold is met or when the maximum number of iterations is reached. In the case of optimizing

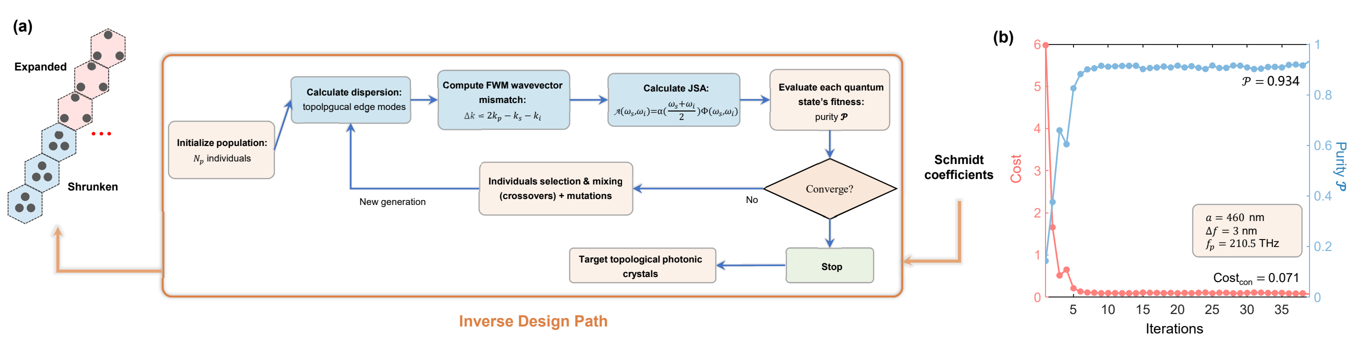

FIG. S1. (a) Schematic of the inverse design method using a GA method.(b) Optimization results of high-purity topological single-photon sources with certain pumping ($f_p = 193.5$ THz, $\Delta f = 5$ nm).

* gqhe@sjtu.edu.cn
† cjiang@sjtu.edu.cn

high-purity topological single-photon sources, our GA approach successfully converges after 41 iterations, achieving a Schmidt number of $K = 1.07$ a single-photon purity of $P = 0.934$ (Fig. S1(b)).

To implement the GA, we integrate the open-source electromagnetic simulation software package MEEP (available at http://ab-initio.mit.edu/meep) with the Distributed Evolutionary Algorithms in Python (DEAP) framework. The optimization process is executed on a computer equipped with an Intel(R) Xeon(R) W-2255 CPU @3.70 GHz and 128 GB of RAM. The GA is initialized with a population size of 50, and the optimization is performed over 100 iterations. The total computational runtime for the inverse design process is approximately 8 hours. Additionally, to monitor the optimization progress, a visual graph of the fitness value evolution is updated after each iteration, allowing real-time tracking of the best fitness improvement throughout the process.

While GA provides a systematic search strategy for optimal design parameters, it suffers from high computational cost due to its reliance on iterative band structure calculations. In contrast, our ML-based inverse design approach offers significant advantages in computational efficiency and scalability. In terms of computational efficiency, GA requires multiple iterations of full-band structure simulations before converging to an optimal solution, leading to a substantial computational burden. The optimization process scales poorly as the number of design parameters increases. In contrast, ML leverages a pre-trained forward neural network to directly map structural parameters to the target properties, eliminating the need for iterative simulations during inverse design. This drastically reduces computational time, improving efficiency by several orders of magnitude. In addition, GA becomes computationally intractable when optimizing structures with a large number of parameters, as the search space grows exponentially. On the other hand, ML-based inverse design scales efficiently to complex structures with multiple design parameters, making it particularly suitable for high-dimensional optimization problems.

II. EXPERIMENTAL REALIZATION OF QUANTUM STATES IN TOPOLOGICAL PHOTONIC CRYSTALS

The fabrication of photonic crystals on silicon-on-insulator (SOI) platforms is well-established in modern nanofabrication [1–5]. In this work, the designed topological devices can be fabricated on an SOI wafer with a 220 nm thick top silicon layer and a 3 µm thick buried silicon layer. The edge coupler, silicon waveguide, and kagome photonic crystal structures are patterned and etched to a depth of 220 nm. A 1 µm thick SiO_2 cladding is subsequently deposited using plasma-enhanced chemical vapor deposition (PECVD). The entire chip is then deeply etched and diced into multiple individual chips. The fabrication process follows standard electron beam lithography (Vistec EBPG 5200+) and inductively coupled plasma (ICP) etching (SPTS DRIE-I) to define high-resolution structures. These well-established fabrication techniques ensure high precision in Refs. [6, 7].

Besides fabrication feasibility, it is also possible to achieve nonlinear optical effects in photonic crystals [8]. Silicon has a third-order nonlinear coefficient ($\chi^{(3)}$), but its nonlinearity is relatively weak. However, this can be enhanced in experiments by using pulsed laser pumping, which allows strong nonlinear interactions in silicon-based photonic crystals [9–11]. Another approach is to use materials with stronger intrinsic nonlinearity, such as lithium niobate, to further enhance the nonlinear response. Therefore, we strongly believe that our proposed topological photonic crystal-based quantum state generation method can be implemented using existing integrated photonic platforms and advanced nanofabrication technology.

[1] M. I. Shalaev, W. Walasik, A. Tsukernik, Y. Xu, and N. M. Litchinitser, Robust topologically protected transport in photonic crystals at telecommunication wavelengths, Nature Nanotechnology **14**, 31 (2019).

[2] C. A. Rosiek, G. Arregui, A. Vladimirova, M. Albrechtsen, B. Vosoughi Lahijani, R. E. Christiansen, and S. Stobbe, Observation of strong backscattering in valley-hall photonic topological interface modes, Nature Photonics **17**, 386 (2023).

[3] X.-T. He, E.-T. Liang, J.-J. Yuan, H.-Y. Qiu, X.-D. Chen, F.-L. Zhao, and J.-W. Dong, A silicon-on-insulator slab for topological valley transport, Nature Communications **10**, 872 (2019).

[4] S. Kiriushechkina, A. Vakulenko, D. Smirnova, S. Guddala, Y. Kawaguchi, F. Komissarenko, M. Allen, J. Allen, and A. B. Khanikaev, Spin-dependent properties of optical modes guided by adiabatic trapping potentials in photonic dirac metasurfaces, Nature Nanotechnology **18**, 875 (2023).

[5] Z. Jiang, H. Wang, P. Xie, Y. Yang, Y. Shen, B. Ji, Y. Chen, Y. Zhang, L. Sun, Z. Wang, *et al.*, On-chip topological transport of integrated optical frequency combs, Photonics Research **13**, 163 (2025).

[6] Y. Su and Y. Zhang, *Passive silicon photonics devices* (American Institute of Physics, 2022).

[7] Y. Su, Y. Zhang, C. Qiu, X. Guo, and L. Sun, Silicon photonic platform for passive waveguide devices: Materials, fabrication, and applications, Advanced Materials Technologies **5**, 1901153 (2020).

[8] J. W. You, Z. Lan, Q. Ma, Z. Gao, Y. Yang, F. Gao, M. Xiao, and T. J. Cui, Topological metasurface: from passive toward active and beyond, Photonics Research **11**, B65 (2023).

[9] D. Smirnova, S. Kruk, D. Leykam, E. Melik-Gaykazyan, D.-Y. Choi, and Y. Kivshar, Third-harmonic generation in photonic topological metasurfaces, Physical review letters **123**, 103901 (2019).
[10] Q. Yuan, L. Gu, L. Fang, X. Gan, Z. Chen, and J. Zhao, Giant enhancement of nonlinear harmonic generation in a silicon topological photonic crystal nanocavity chain, Laser & Photonics Reviews **16**, 2100269 (2022).
[11] S. S. Kruk, W. Gao, D.-Y. Choi, T. Zentgraf, S. Zhang, and Y. Kivshar, Nonlinear imaging of nanoscale topological corner states, Nano letters **21**, 4592 (2021).